# Analytical shock solutions at large and small Prandtl number

B. M. Johnson

March 20, 2013

**Disclaimer**

This document was prepared as an account of work sponsored by an agency of the United States government. Neither the United States government nor Lawrence Livermore National Security, LLC, nor any of their employees makes any warranty, expressed or implied, or assumes any legal liability or responsibility for the accuracy, completeness, or usefulness of any information, apparatus, product, or process disclosed, or represents that its use would not infringe privately owned rights. Reference herein to any specific commercial product, process, or service by trade name, trademark, manufacturer, or otherwise does not necessarily constitute or imply its endorsement, recommendation, or favoring by the United States government or Lawrence Livermore National Security, LLC. The views and opinions of authors expressed herein do not necessarily state or reflect those of the United States government or Lawrence Livermore National Security, LLC, and shall not be used for advertising or product endorsement purposes.

# Analytical shock solutions at large and small Prandtl number

## B. M. Johnson[1]†

[1]Lawrence Livermore National Laboratory, Livermore, CA 94550, USA

Exact one-dimensional solutions to the equations of fluid dynamics are derived in the $Pr \to \infty$ and $Pr \to 0$ limits (where $Pr$ is the Prandtl number). The solutions are analogous to the $Pr = 3/4$ solution discovered by Becker and analytically capture the profile of shock fronts in ideal gases. The solutions consist of implicit expressions for the fluid variables and can incorporate a temperature- and density-dependent viscosity or thermal conductivity. The large-$Pr$ solution is very similar to the Becker solution, differing only by a scale factor. The small-$Pr$ solution is qualitatively different, with an embedded isothermal shock occurring above a critical Mach number, analogous to the embedded discontinuity that occurs in radiative shocks. In fact, for a conductivity that varies as the cube of the temperature, the small-$Pr$ solution yields analytical expressions for the fluid variables in the low-energy density, constant opacity, grey equilibrium diffusion limit of radiation hydrodynamics. Analytical solutions are also derived for a viscosity and conductivity with a general power-law temperature and density dependence. The maximum error in the analytical solutions when compared to a numerical integration of the finite-$Pr$ equations is $O\left(Pr^{-1}\right)$ as $Pr \to \infty$ and $O(Pr)$ as $Pr \to 0$.

**Key words:**

---

## 1. Introduction

Although the power of numerical techniques makes them indispensable for solving the equations of fluid dynamics, analytical solutions, while often difficult to find, remain useful for several reasons. They build physical intuition, they can be quickly evaluated over a wide dynamic range, and they can be used to verify numerical algorithms. One such solution was discovered by Becker (1922, see also Morduchow & Libby 1949; Zel'dovich & Raizer 2002) under the assumptions of a steady-state, one planar dimension, constant viscosity, and a fluid Prandtl number of 3/4. It gives implicit, closed-form expressions for the fluid variables and analytically captures the behavior of shocks in ideal gases with $Pr = 3/4$. It is shown here that analogous solutions can be derived in both the $Pr \to \infty$ and $Pr \to 0$ limits, and that the solutions in all three limits can be extended to non-constant viscosity or thermal conductivity. These solutions yield analytical profiles of shock fronts in ideal gases over a wide range of parameter space. The basic equations are outlined in §2, §3 gives the derivation of the solutions, and §4 discusses some implications.

† Email address for correspondence: johnson359@llnl.gov

## 2. Basic equations

For a fluid with mass density $\rho$, velocity magnitude $v$, pressure $p$, internal energy $e$, temperature $T$, viscosity $\mu$ and thermal conductivity $\kappa$ ($Pr = \mu C_p/\kappa$, where $C_p$ is the specific heat at constant pressure), the equations of fluid dynamics in planar geometry are:

$$\frac{\partial \rho}{\partial t} + \frac{\partial}{\partial x}(\rho v) = 0, \tag{2.1}$$

$$\frac{\partial}{\partial t}(\rho v) + \frac{\partial}{\partial x}\left(\rho v^2 + p - \frac{4\mu}{3}\frac{\partial v}{\partial x}\right) = 0, \tag{2.2}$$

$$\frac{\partial}{\partial t}\left(\frac{1}{2}\rho v^2 + \rho e\right) + \frac{\partial}{\partial x}\left(\rho v\left[\frac{1}{2}v^2 + h\right] - \frac{4\mu}{3}v\frac{\partial v}{\partial x} - \kappa\frac{\partial T}{\partial x}\right) = 0, \tag{2.3}$$

where $h = p + \rho e$ is the fluid enthalpy (Landau & Lifshitz 1987). It will be assumed throughout that the fluid obeys an ideal gas equation of state:

$$p = (\gamma - 1)\rho e,$$

so that $h = \gamma e = C_p T$ with $C_p = \gamma C_v$, where $C_v$ is the specific heat at constant volume. Under this assumption and the assumption of a steady-state, equations 2.1–2.3 can be integrated once to give:

$$\rho v = \rho_0 v_0 \equiv m_0, \tag{2.4}$$

$$v^2 + \frac{\gamma - 1}{\gamma}h - \frac{4\mu}{3m_0}v\frac{dv}{dx} = \left(v_0^2 + \frac{\gamma - 1}{\gamma}h_0\right)\frac{\rho_0}{\rho}, \tag{2.5}$$

$$\frac{1}{2}v^2 + h - \frac{4\mu}{3\rho}\frac{dv}{dx} - \frac{\kappa}{\rho v C_p}\frac{dh}{dx} = \left(\frac{1}{2}v_0^2 + h_0\right)\frac{\rho_0 v_0}{\rho v}, \tag{2.6}$$

where the zero-slope boundary conditions appropriate for a shock have been chosen at $x = \pm\infty$. A subscript "0" here denotes a fluid quantity in the ambient (pre-shock) state. These equations can be combined into two ordinary differential equations governing the spatial profile of the shock front:

$$\frac{4\mu}{3m_0}v\frac{dv}{dx} = v^2 + \frac{\gamma - 1}{\gamma}h - \frac{\gamma + 1}{2\gamma}(v_0 + v_1)v, \tag{2.7}$$

$$\frac{\kappa}{m_0 C_p}\frac{dh}{dx} = \frac{h}{\gamma} - \frac{v^2}{2} + \frac{\gamma + 1}{2\gamma}(v_0 + v_1)v - \frac{\gamma + 1}{\gamma - 1}\frac{v_0 v_1}{2}, \tag{2.8}$$

where the integration constants have been expressed in terms of both pre-shock and post-shock (denoted by a subscript "1") velocities via the Rankine-Hugoniot jump conditions. Here

$$v_1 = v_0\frac{\gamma - 1 + 2/M_0^2}{\gamma + 1}, \tag{2.9}$$

where $M_0^2 = v_0^2/c_0^2$ is the shock Mach number and $c_0 = \sqrt{\gamma p_0/\rho_0}$ is the adiabatic sound speed in the ambient fluid (Landau & Lifshitz 1987).

## 3. Solutions

The derivation of the Becker (1922) solution is outlined in §3.1, followed by a derivation of the $Pr \to \infty$ and $Pr \to 0$ solutions in §3.2 and §3.3, respectively. These are all derived for constant viscosity and conductivity; §3.4 shows how the solutions can be extended to non-constant viscosity and conductivity, using the grey equilibrium diffusion limit of

radiation hydrodynamics as an example. General expressions for the shock profiles in all three $Pr$ limits under the assumption of a viscosity and conductivity that vary as powers of the density and temperature are derived in §3.5.

### 3.1. *Becker* $(Pr = 3/4)$ *solution*

Becker (1922) noticed that for $Pr = 3/4$ equation 2.6 for the energy flux,

$$\frac{v^2}{2} + h - \frac{\kappa}{m_0 C_p} \frac{d}{dx} \left( \frac{v^2}{2} + h \right) = \frac{v_0^2}{2} + h_0, \tag{3.1}$$

is linear and has the finite solution

$$\frac{v^2}{2} + h = \frac{v_0^2}{2} + h_0 = \frac{\gamma + 1}{\gamma - 1} \frac{v_0 v_1}{2}, \tag{3.2}$$

where the second equality follows from the Rankine-Hugoniot conditions. Solving this equation for $h$ and inserting it into equation 2.5 for the momentum flux leads to

$$v L_\kappa \frac{dv}{dx} = \frac{\gamma + 1}{2} \left( v - v_0 \right) \left( v - v_1 \right), \tag{3.3}$$

where

$$L_\kappa \equiv \frac{\kappa_0}{m_0 C_v}$$

and $\kappa = \kappa_0$ is assumed here to be spatially constant. Equation 3.3 can be rewritten as an integral over the velocity,

$$x = \frac{2 L_\kappa}{\gamma + 1} \int \frac{v}{\left( v - v_0 \right) \left( v - v_1 \right)} \, dv.$$

To within an arbitrary constant, this integral is given by

$$x = \frac{2 L_\kappa}{\gamma + 1} \ln \left[ \left( v_0 - v \right)^{\frac{v_0}{v_0 - v_1}} \left( v - v_1 \right)^{-\frac{v_1}{v_0 - v_1}} \right]. \tag{3.4}$$

Physical notation has been retained here as an aid to intuition; notice that $x = \pm \infty$ at $v = v_1$ and $v = v_0$, respectively. Defining the origin at the adiabatic sonic point $\left( v = \sqrt{v_0 v_1} \right)$ and using $\eta \equiv v/v_0$ rather than $v$ yields the expression given in Zel'dovich & Raizer (2002). From 3.2, the temperature in this limit is given by

$$\frac{T}{T_0} = \frac{\gamma - 1}{2} M_0^2 \left( R_\infty \eta_1 - \eta^2 \right), \tag{3.5}$$

where

$$R_\infty \equiv \frac{\gamma + 1}{\gamma - 1}$$

is the maximum compression ratio. Having an expression for the temperature in terms of $\eta$ will be useful in §3.5.

Figure 1 shows the velocity and temperature for this solution, using expressions 3.4 and 3.5. For comparison, results from a numerical integration of equations 2.7 and 2.8 are shown in figure 1 as well. The numerical results here and in the following sections were obtained via a shooting method using the `odeint` differential equation solver in `scipy`. An important practical note here is that it is necessary to shoot from the post-shock state in order to obtain the desired solution. Equation 3.1 admits an exponential solution in addition to the constant solution (the right-hand side of equation 3.2), representing an additional energy flux at the boundary of arbitrary magnitude (Zel'dovich & Raizer 2002). For an integration from the pre- to post-shock state, this solution is exponentially
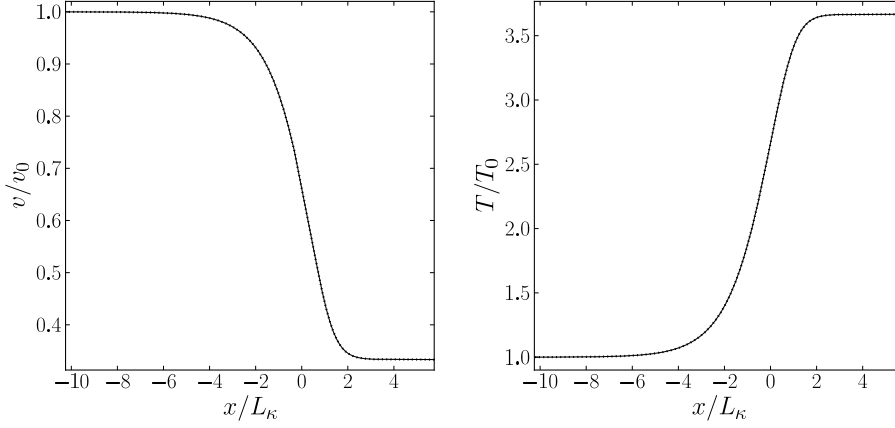
FIGURE 1. Velocity (*left*) and temperature (*right*) for the Becker solution ($Pr = 3/4$) with $M_0 = 3$. Solid lines are analytical results, dotted lines are numerical results.

growing, bounded only by the end point of the integration, and can quickly dominate the numerical results. For an integration from the post- to pre-shock state, the exponential solution is decaying and therefore unproblematic.

### 3.2. *Large-Pr solution*

In the limit $Pr \to \infty$ ($\kappa \to 0$), equations 2.5 and 2.6 become

$$v^2 + \frac{\gamma - 1}{\gamma} h - \frac{4\mu}{3m_0} v \frac{dv}{dx} = \frac{\gamma + 1}{2\gamma} (v_0 + v_1) v, \tag{3.6}$$

$$\frac{1}{2} v^2 + h - \frac{4\mu}{3m_0} v \frac{dv}{dx} = \frac{\gamma + 1}{\gamma - 1} \frac{v_0 v_1}{2}, \tag{3.7}$$

which can be combined to give

$$v L_\mu \frac{dv}{dx} = \frac{\gamma + 1}{2} (v - v_0) (v - v_1), \tag{3.8}$$

where

$$L_\mu \equiv \frac{4\mu_0}{3m_0} = \frac{4Pr}{3\gamma} L_\kappa$$

and $\mu = \mu_0$ is assumed here to be spatially constant. This can again be expressed as an integral over velocity,

$$x = \frac{2L_\mu}{\gamma + 1} \int \frac{v}{(v - v_0)(v - v_1)} \, dv,$$

with the solution given by

$$x = \frac{2L_\mu}{\gamma + 1} \ln \left[ (v_0 - v)^{\frac{v_0}{v_0 - v_1}} (v - v_1)^{-\frac{v_1}{v_0 - v_1}} \right]. \tag{3.9}$$

Comparing expression 3.9 with 3.4, it can be seen that the velocity profile in the large-*Pr* solution differs from that of the Becker (1922) solution only by the scale factor $L_\mu / L_\kappa = 4Pr/(3\gamma)$. The difference between the temperature profiles is more complicated, since solving equations 3.6 and 3.7 for the temperature in this limit yields an expression that differs from expression 3.5:

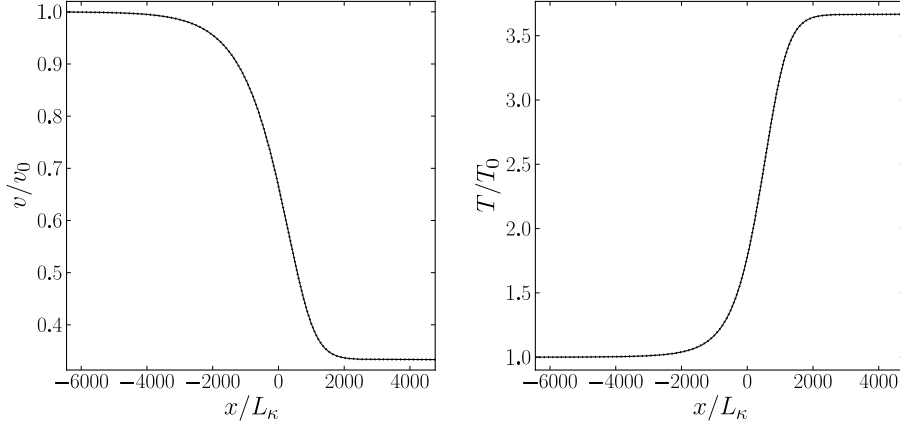$$\frac{T}{T_0} = \frac{\gamma (\gamma - 1)}{2} M_0^2 \left( \eta^2 - 4\eta_i \eta + R_\infty \eta_1 \right), \tag{3.10}$$

FIGURE 2. Velocity (*left*) and temperature (*right*) for the $Pr \to \infty$ solution with $M_0 = 3$ and constant viscosity. Solid lines are analytical results, dotted lines are numerical results.

where

$$\eta_i \equiv \frac{\gamma + 1}{4\gamma} \left(1 + \eta_1\right). \tag{3.11}$$

Figure 2 shows the velocity and temperature for the large-$Pr$ solution with $M_0 = 3$ and constant viscosity. A value of $Pr = 10^3$ was used to generate the numerical results in this figure.

### 3.3. *Small-Pr solution*

In the limit $Pr \to 0$ ($\mu \to 0$), equations 2.5 and 2.6 become

$$v^2 + \frac{\gamma - 1}{\gamma} h = \frac{\gamma + 1}{2\gamma} \left(v_0 + v_1\right) v, \tag{3.12}$$

$$\frac{v^2}{2} + h - \frac{\kappa}{m_0 C_p} \frac{dh}{dx} = \frac{\gamma + 1}{\gamma - 1} \frac{v_0 v_1}{2}. \tag{3.13}$$

Taking the spatial derivative of 3.12 and eliminating the enthalpy derivative via 3.13 and the enthalpy via 3.12 gives

$$2 \left(v - v_i\right) L_\kappa \frac{dv}{dx} = \frac{\gamma + 1}{2} \left(v - v_0\right) \left(v - v_1\right), \tag{3.14}$$

where

$$v_i = v_0 \eta_i$$

is the velocity at the isothermal sonic point, $v = c_i = \sqrt{p/\rho}$ ($v_i$ is the isothermal sonic point only for the small-$Pr$ solution). Notice that unlike equations 3.3 and 3.8, equation 3.14 is singular at $v = v_i$. Expressed as an integral over the velocity,

$$x = \frac{4L_\kappa}{\gamma + 1} \int \frac{v - v_i}{\left(v - v_0\right) \left(v - v_1\right)} dv,$$

a full solution can be obtained for $x(v)$ (valid to within an arbitrary constant):

$$x = \frac{4L_\kappa}{\gamma \left(\gamma + 1\right)} \ln \left[\left(v_0 - v\right)^{\frac{\beta v_0 - v_1}{v_0 - v_1}} \left(v - v_1\right)^{\frac{v_0 - \beta v_1}{v_0 - v_1}}\right], \tag{3.15}$$

where

$$\beta \equiv \frac{3\gamma - 1}{\gamma + 1}.$$

From 3.12, the temperature in this limit is given by

$$\frac{T}{T_0} = \gamma M_0^2 \eta \left(2\eta_i - \eta\right). \tag{3.16}$$

Despite appearances, the singularity in equation 3.14 has not been avoided. It is clear from 3.14 that $dx/dv = 0$ at $v = v_i$, and it is straightforward to show that $x$ is a maximum here for $v_1 < v_i < v_0$ (i.e., if the singularity lies within the shock region). The solution 3.15 is thus double-valued when regarded as a solution for $v(x)$. Since 3.15 remains valid under the transformation $x \to -x, v \to -v$, a solution for $v(x)$ can be patched together by spatially reversing the portion of the solution with $v < v_i$. The resulting solution is continuous and exhibits a temperature spike in a manner analagous to the Zel'dovich spike that occurs in radiative shocks (Zel'dovich & Raizer 2002; Mihalas & Mihalas 1984). However, the solution suffers from an infinite velocity derivative at $v = v_i$, indicating that viscosity must be important in this region. Numerical integration of equations 2.7 and 2.8 shows that the regularization due to viscosity results in an embedded isothermal shock, with the velocity dropping rapidly to $v_1$ as soon as the precursor temperature reaches $T_1$. This occurs for

$$\frac{T_1}{T_0} = \gamma M_0^2 \eta \left(2\eta_i - \eta\right) = \gamma M_0^2 \eta_1 \left(2\eta_i - \eta_1\right). \tag{3.17}$$

Equation 3.17 can be rewritten as $\left(\eta - \eta_1\right)\left(\eta - 2\eta_i + \eta_1\right) = 0$, indicating that $T = T_1$ at both $v = v_1$ and

$$v = 2v_i - v_1.$$

If the singularity lies within the shock region $(v_i > v_1)$, the small-$Pr$ solution is given by expression 3.15 for $2v_i - v_1 < v < v_0$, followed by an isothermal shock from $v = 2v_i - v_1$ to $v = v_1$. For $v_i < v_1$, or

$$M_0 < \sqrt{\frac{3\gamma - 1}{\gamma\left(3 - \gamma\right)}}, \tag{3.18}$$

the solution is continuous and given by expression 3.15 throughout the shock region. Figure 3 shows the velocity and temperature for the small-$Pr$ solution with $M_0 = 3$ and constant conductivity. A value of $Pr = 10^{-3}$ was used to generate the numerical results in this figure. The solution is discontinuous in this case.

### 3.4. *Grey equilibrium diffusion*

The character of the solutions described in the previous section is reminiscent of radiative shock solutions in the grey equilibrium diffusion limit (Lowrie & Rauenzahn 2007, and references therein). For a constant opacity, diffusive radiation behaves as a thermal conductivity with a $T^3$ dependence:

$$\kappa = \frac{16T^3\sigma}{3\chi},$$

where $\sigma$ is the Stefan-Boltzmann constant and $\chi$ is the opacity in units of inverse length. Equation 3.14 in that case can be expressed as

$$x = \frac{4L_\kappa}{\gamma + 1} \int \left(\frac{T}{T_0}\right)^3 \frac{v - v_i}{\left(v - v_0\right)\left(v - v_1\right)} dv,$$
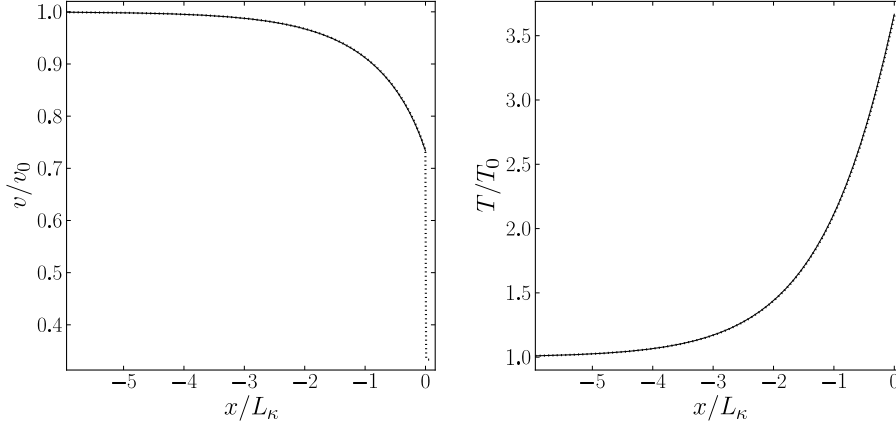
FIGURE 3. Velocity (*left*) and temperature (*right*) for the $Pr \rightarrow 0$ solution with $M_0 = 3$ and constant conductivity. Solid lines are analytical results, dotted lines are numerical results.

with $\kappa_0 = 16T_0^3 \sigma/(3\chi)$. Using equation 3.16, this can be rewritten as

$$x = \frac{4L_\kappa \gamma^3 M_0^6}{\gamma + 1} \int \frac{\eta^3 (2\eta_i - \eta)^3 (\eta - \eta_i)}{(\eta - 1)(\eta - \eta_1)} d\eta. \tag{3.19}$$

The integrand in the above expression can be expanded into

$$\frac{\eta^3 (2\eta_i - \eta)^3 (\eta - \eta_i)}{(\eta - 1)(\eta - \eta_1)} = \frac{\eta^6 + c_1 \eta^5 + c_2 \eta^3}{\eta - 1} + \frac{-2\eta^6 + c_3 \eta^5 + c_4 \eta^3}{\eta - \eta_1},$$

where

$$c_1 \equiv \frac{7\eta_i + \eta_1 - 2 - 18\eta_i^2}{1 - \eta_1}, \quad c_2 \equiv \frac{4\eta_i^3 (2\eta_i - 5)}{\eta_1 - 1},$$

$$c_3 \equiv \frac{-7\eta_i \eta_1 - \eta_1^2 + 2\eta_1 + 18\eta_i^2}{1 - \eta_1}, \quad c_4 \equiv \frac{4\eta_i^3 (5\eta_1 - 2\eta_i)}{\eta_1 - 1}.$$

Using the result (for integer $m$)

$$\int \frac{z^n}{z - c} dz = c^n \ln(z - c) + \sum_{m=1}^{n} c^{n-m} \frac{z^m}{m},$$

the integral in expression 3.19 is given by

$$\int \frac{\eta^3 (2\eta_i - \eta)^3 (\eta - \eta_i)}{(1 - \eta)(\eta - \eta_1)} d\eta = \ln(1 - \eta)^{\alpha_1} + \ln(\eta - \eta_1)^{-\alpha_2}$$

$$+ \sum_{m=1}^{6} \left(1 - 2\eta_1^{6-m}\right) \frac{\eta^m}{m} + \sum_{m=1}^{5} \left(c_1 + c_3 \eta_1^{5-m}\right) \frac{\eta^m}{m} + \sum_{m=1}^{3} \left(c_2 + c_4 \eta_1^{3-m}\right) \frac{\eta^m}{m}, \tag{3.20}$$

where

$$\alpha_1 \equiv \frac{(\eta_i - 1)(2\eta_i - 1)^3}{\eta_1 - 1}, \quad \alpha_2 \equiv \frac{\eta_1^3 (\eta_i - \eta_1)(2\eta_i - \eta_1)^3}{\eta_1 - 1}.$$

Combining this result with expression 3.19 gives a closed form expression for $x(v)$. An alternative expression in terms of transcendental functions is given in §3.5; the above expression, albeit complicated, is straightforward to implement numerically in terms of elementary functions.
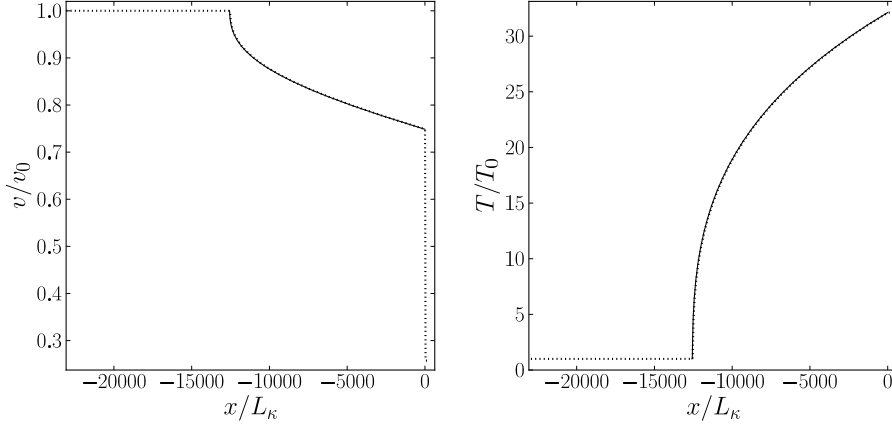
FIGURE 4. Velocity (*left*) and temperature (*right*) for the $Pr \to 0$ solution with $M_0 = 10$ and $\kappa \sim T^3$. Solid lines are analytical results, dotted lines are numerical results.
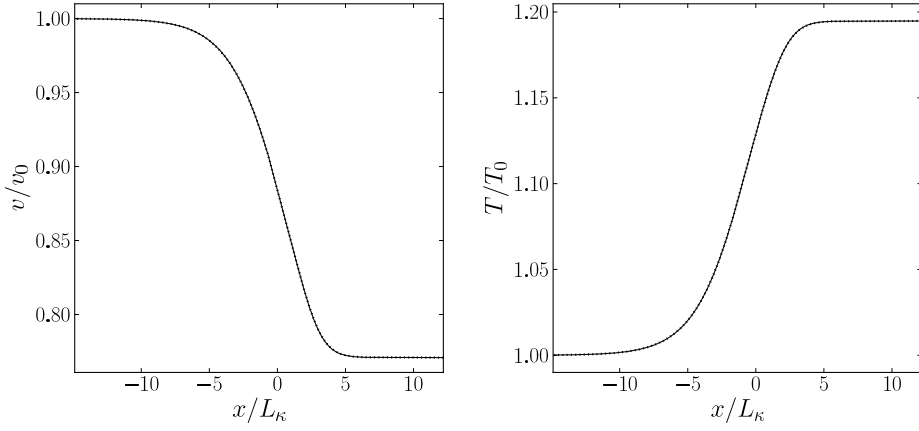


FIGURE 5. Velocity (*left*) and temperature (*right*) for the $Pr \to 0$ solution with $M_0 = 1.2$ and $\kappa \sim T^3$. Solid lines are analytical results, dotted lines are numerical results.

Figures 4 and 5 show the velocity and temperature for the solution described in this section with $M_0 = 10$ and $M_0 = 1.2$, respectively. A value of $Pr = 10^{-4}$ was used to generate the numerical results in these figures. Compare with figures 3 and 5 of Lowrie & Rauenzahn (2007). Notice that $\eta_i \to 1/2$ as $M_0 \to \infty$ (from 2.9 and 3.11), so that $\alpha_1 \to 0$ and the $\ln(1 - \eta)$ term in 3.20 is negligible at large Mach number. This accounts for the slope discontinuity at the leading edge of the precursor in figure 4.

### 3.5. *Power-law viscosity and conductivity*

For a viscosity and thermal conductivity that vary as a power-law in density and temperature,

$$\mu = \mu_0 \left(\frac{\rho}{\rho_0}\right)^a \left(\frac{T}{T_0}\right)^b, \quad \kappa = \kappa_0 \left(\frac{\rho}{\rho_0}\right)^a \left(\frac{T}{T_0}\right)^b,$$

the solutions to equations 3.3, 3.8 and 3.14 are

$$x\left(Pr = 3/4\right) = \frac{2L_\kappa}{\gamma + 1} \left(\frac{[\gamma - 1] M_0^2}{2}\right)^b \int \frac{\eta^{1-a} \left(R_\infty \eta_1 - \eta^2\right)^b}{(\eta - 1)(\eta - \eta_1)} \, d\eta, \qquad (3.21)$$

$$x\,(Pr=\infty) = \frac{2L_\mu}{\gamma+1}\left(\frac{\gamma\,[\gamma-1]\,M_0^2}{2}\right)^b \int \frac{\eta^{1-a}\left(\eta^2-4\eta_i\eta+R_\infty\eta_1\right)^b}{(\eta-1)\,(\eta-\eta_1)}\,d\eta, \qquad (3.22)$$

$$x\,(Pr=0) = \frac{4L_\kappa}{\gamma+1}\left(\gamma M_0^2\right)^b \int \frac{(\eta-\eta_i)\,\eta^{b-a}\,(2\eta_i-\eta)^b}{(\eta-1)\,(\eta-\eta_1)}\,d\eta, \qquad (3.23)$$

where expressions 3.5, 3.10 and 3.16, respectively, have been used for $T/T_0$. The problem has thus been reduced to quadrature under quite general conditions. Expression 3.23, along with expressions 3.21 and 3.22 for particular values of $a$ and $b$, can be expressed in terms of Appell functions, although these can be slow to evaluate numerically. For example, the small-$Pr$ solution for general $a$ and $b$ is

$$\begin{aligned}
x\,(Pr=0) = {}& \frac{4L_\kappa\left(2\gamma M_0^2\right)^b v_0}{(\gamma+1)\,(b-a+1)\,(v_0-v_1)}\left(\frac{v_i}{v_0}\right)^b\left(\frac{v}{v_0}\right)^{b-a+1}\\
&\times\left(\left[\frac{v_i}{v_0}-1\right]F_1\left[b-a+1;-a,1;b-a+2;\frac{v}{2v_i},\frac{v}{v_0}\right]\right.\\
&\left.+\left[1-\frac{v_i}{v_1}\right]F_1\left[b-a+1;-a,1;b-a+2;\frac{v}{2v_i},\frac{v}{v_1}\right]\right),\qquad (3.24)
\end{aligned}$$

where $F_1$ is the Appell function of the first kind. Analytical expressions in terms of elementary functions can be obtained for particular values of $a$ and $b$ (the solution in §3.4 is an example with $a=0$, $b=3$), although they can be quite lengthy. The expression for a Spitzer conductivity ($a=0$, $b=5/2$), for example, is even longer than expression 3.20 and is not reproduced here. The best approach for general $a$ and $b$ is to perform the quadratures in 3.21–3.23 numerically. Notice that $\mu$ and $\kappa$ have been assumed to have the same temperature and density dependence so that $Pr$ is constant, for simplicity; this assumption is not necessary and is easily relaxed.

## 4. Discussion

Exact solutions to the equations of fluid dynamics have been derived in the $Pr\to\infty$ and $Pr\to0$ limits, analogous to the $Pr\to3/4$ solution derived by Becker (1922). For finite $Pr$, the solutions are accurate to within $Pr^{-1}$ for $Pr\to\infty$ and $Pr$ for $Pr\to0$ (see figure 6). The solutions have been shown to extend to non-constant viscosity and conductivity, in particular for a power-law dependence in temperature and density, although further extensions not elaborated here are possible (such as for a Sutherland viscosity). The derived solutions are given in their most general form by expressions 3.21–3.23, with specific forms for a constant viscosity and conductivity given by expressions 3.4, 3.9 and 3.15. An alternative form of 3.23 is given by expression 3.24.

A small-$Pr$ solution with a $T^3$ dependence has also been derived (expressions 3.19 and 3.20) that is equivalent to the semi-analytical solutions of Lowrie & Rauenzahn (2007) for grey equilibrium diffusion in the low-energy density limit (in the notation of Lowrie & Rauenzahn 2007, this is the $\mathcal{P}_0\to0$ limit, where $\mathcal{P}_0$ is approximately the ratio of radiation to material pressures). Since the equilibrium solution for radiative shocks is in many cases a good approximation to the more physically-relevant non-equilibrium solution (i.e., where the radiation and material temperatures are out of equilibrium, see Lowrie & Edwards 2008), expressions 3.19 and 3.23 provide a good estimate of the width of radiative shocks, the former for the constant opacity case, and the latter for non-constant opacity (in that case, simply make the substitution $a=-a'-1$ and $b=3-b'$, where $a'$ and $b'$ are the density and temperature power-laws, respectively, for the opacity expressed in units of area per mass). Notice that the width of a radiative shock precursor
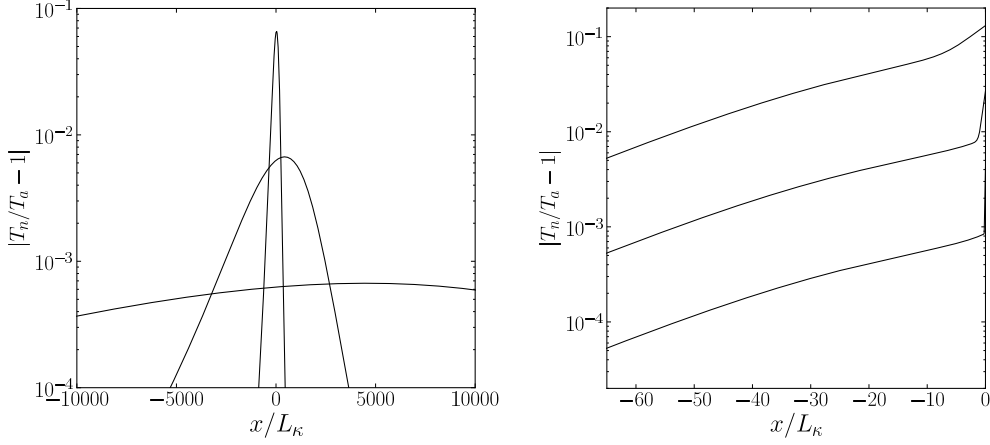
FIGURE 6. Temperature errors in the large-$Pr$ (*left*) and small-$Pr$ (*right*) solutions with constant viscosity and conductivity (figures 2 and 3), for (from *top* to *bottom*) $Pr = 10, 100, 1000$ (*left*) and $Pr = 0.1, 0.01, 0.001$ (*right*).

can be quite sensitive to the shock Mach number ($x \sim M_0^6$ in the case of a constant opacity).

In addition to providing physical insight, the analytical solutions derived here are useful for quickly evaluating shock profiles over a wide range of parameter space. It is possible to comprehend at a glance the scaling of the solutions with various parameters without resorting to a comprehensive parameter survey via numerical integration. The solutions are also nonlinear, with the only assumptions behind their derivation being a steady-state, one planar dimension, and an ideal gas equation of state. In particular, no terms in the evolution equations have been approximated, which makes these solutions an excellent verification test for numerical algorithms.

## REFERENCES

BECKER, R. 1922 Stosswelle und Detonation. *Z. Physik.* **8**, 321–362.

LANDAU, L. D. & LIFSHITZ, E. M. 1987 *Fluid Mechanics.* Butterworth–Heinemann.

LOWRIE, R. B. & EDWARDS, J. D. 2008 Radiative shock solutions with grey nonequilibrium diffusion. *Shock Waves.* **18**, 129–143.

LOWRIE, R. B. & RAUENZAHN, R. M. 2007 Radiative shock solutions in the equilibrium diffusion limit. *Shock Waves.* **16**, 445–453.

MIHALAS, D. & MIHALAS, B. W. 1984 *Foundations of Radiation Hydrodynamics.* Oxford University Press.

MORDUCHOW, M. & LIBBY, P. A. 1949 On a complete solution of the one-dimensional flow equations of a viscous, heat conducting, compressible gas. *J. Aeron. Sci.* **16**, 674–684.

ZEL'DOVICH, YA. B. & RAIZER, YU. P. 2002 *Physics of Shock Waves and High-Temperature Hydrodynamic Phenomena.* Dover.